Best of Both Modalities: Fusing CBCT and Intraoral Scan Data into a Single Tooth Image

SaeHyun Kim[1(*)], Yongjin Choi[1(*)], Jincheol Na[1], In-Seok Song[2], You-Sun Lee[2], Bo-Yeon Hwang[2], Ho-Kyung Lim[2], and Seung Jun Baek[1(✉)]

[1] Korea University, Seoul, South Korea
{vnv73, dydwls8445, wlscjf736, sjbaek}@korea.ac.kr
[2] Korea University Anam Hospital, Seoul, South Korea
{densis, kumc_ortho, bo0426, ungassi}@korea.ac.kr

Abstract. Cone-Beam CT (CBCT) and Intraoral Scan (IOS) are dental imaging techniques widely used for surgical planning and simulation. However, the spatial resolution of crowns is low in CBCT, and roots are not visible in IOS. We propose to take the best of both modalities: a seamless fusion of the crown from IOS and the root from CBCT into a single image in a watertight mesh, unlike prior works that compromise the resolution or simply overlay two images. The main challenges are aligning two images (registration) and fusing them (stitching) despite a large gap in the spatial resolution between two modalities. For effective registration, we propose centroid matching followed by coarse- and fine-registration based on the point-to-plane ICP method. Next, stitching of registered images is done to create a watertight mesh, for which we recursively interpolate the boundary points to seamlessly fill the gap between the registered images. Experiments show that the proposed method incurs low registration error, and the fused images are of high quality and accuracy according to the evaluation by experts.

Keywords: Intraoral Scan (IOS) · Cone-Beam Computed Tomography (CBCT) · Modality Fusion · Registration · Mesh Stitching

1 Introduction

The 3D visualization of teeth can assist with dental treatment planning [9,12] as well as pre-operational simulation of surgeries [16,21,22]. Cone-beam computed tomography (CBCT) and intraoral scan (IOS) are 3D imaging techniques widely used in such applications. CBCT provides information on dental and maxillofacial structures, whereas IOS provides highly accurate surface information on tooth crowns and gingiva.

While providing comprehensive visualization, CBCT and IOS have their shortcomings. The spatial resolution of crowns represented by CBCT is relatively low, and the roots buried in the gingiva are not visible in IOS. In this

[*] Equal contribution
[✉] Corresponding author

paper, we leverage the strengths of both modalities: fusing the crown from IOS and the root from CBCT into a single tooth image in a watertight mesh. Firstly, the fusion requires aligning CBCT and IOS images of a patient, i.e., *registration*. Next, the registered images need to be combined, for which we need the *stitching* of images. The technical challenges are such that, CBCT and IOS are heterogeneous modalities, e.g., the spatial resolution of IOS tends to be much higher than CBCT. Due to the differences, naive registration and stitching methods tend to perform poorly. Thus, previous attempts at modality fusion simply *overlay* two images, or compromise the resolution of IOS; a detailed review is as follows.

Most studies on integrating CBCT and IOS data focus on registration. Initial attempts of registration utilized fiducial markers [10, 23, 24, 26] which, however, demanded significant manual intervention. Deferm *et al.* [6] focused on registration based on soft tissues rather than dental structures. Common techniques to align dental regions include Principal Component Analysis (PCA) [29] and the Iterative Closest Point (ICP) algorithm [1]. Some enhancements were made for registration, including deep pose regression [2], facial scans [13], and Fast Point Feature Histograms (FPFH)-based ICP [14]. However, the above methods are limited to registration, and the output is a simple overlay of two images. Only a few works attempted to produce a single output mesh, however, at the cost of compromising the resolution. Hao *et al.* [11], and Liu *et al.* [17] output a single image by retaining only the point cloud, and then reconstructing the mesh; but this process risks compromising the fine details originally captured by IOS. Qian *et al.* [20] also performed registration and stitching of IOS and CBCT meshes which, however, suffered from incomplete stitching when the spatial resolution of IOS is much higher than CBCT, which is the usual case.

In this paper, we investigate the multimodal fusion of CBCT and IOS into a unified output to fully exploit the complementary aspects of the two modalities. We first propose an effective registration consisting of three stages: centroid alignment, coarse- and fine-grained registration based on a robust ICP method. Next, we propose a novel method for mesh stitching to combine the registered IOS and CBCT into a watertight mesh, which recursively interpolates the boundary points to seamlessly fill the gap between the registered images. Experiments show that our method incurs low registration errors, and the fused outputs are of high quality and accuracy for clinical usage as evaluated by medical experts. To our belief, our work is the first to integrate CBCT and IOS data into clinically accurate and cohesive meshes without compromising the spatial resolution.

2 Method

2.1 Overview

The proposed method consists of (i) IOS-CBCT registration; (ii) crown removal from CBCT; (iii) mesh stitching. The inputs to our method are pre-segmented IOS and CBCT meshes in which each tooth is individually segmented as its tooth number. Note that several methods are available for such segmentation [3–5, 15, 25, 27, 28]. An overview of our method is illustrated in Fig. 1.

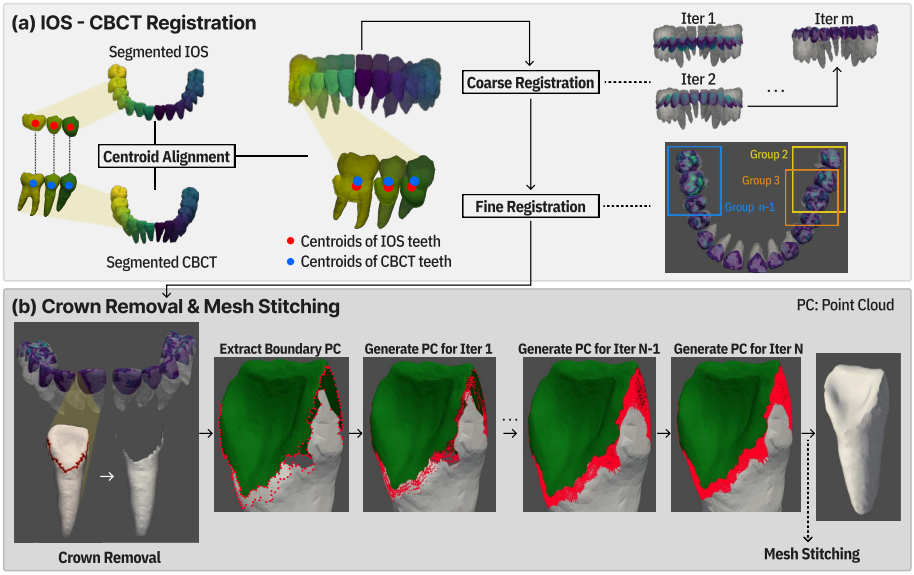

Fig. 1. Overview of Integration of IOS and CBCT images

2.2 IOS-CBCT Registration

The IOS-CBCT registration involves aligning the crown portion of CBCT and IOS. We propose a fine-grained registration consisting of three stages: **1) Centroid Alignment**, **2) Coarse Registration**, and **3) Fine Registration**.

1) Centroid Alignment: Let $X_1, X_2, ..., X_n$ denote the collection of point sets (mesh vertices) from CBCT meshes where X_i denotes the point set of the tooth number i. Similarly define $Y_1, \ldots, Y_n$ for IOS data. We would like to align X_i and Y_i for $i = 1, \ldots, n$. We first perform a gross alignment before refined registration. For initial alignment, we propose a simple yet effective method called centroid alignment as follows. The centroids of CBCT and IOS point sets are calculated, and let C_{X_i} (resp. C_{Y_i}) denote the centroid of the point set of i-th tooth in CBCT (resp. IOS) data. We find transformation R^{cent} through which C_{X_i} and C_{Y_i} are matched for $i = 1, \ldots, n$:

$$R^{\text{cent}} = \arg\min_{R} \sum_{i=1}^{n} \|C_{Y_i} - R(C_{X_i})\|^2 \tag{1}$$

where R denotes a rigid transform matrix. The centroids from both modalities tend to be distributed along the dental arches. Thus, this is a computationally efficient way of roughly aligning the modalities on an overall scale.

2) Coarse Registration: After centroid alignment, the meshes will overlap but crowns may be misaligned (Fig. 1 (a)). The ICP algorithm [1] can be used for a refined registration. Previous works attempted to apply ICP to all teeth using correspondences based on features such as FPFH [14]. However, techniques like

FPFH feature matching may fail due to a mismatch between IOS and CBCT resolutions. Instead, we perform coarse- and fine-registration based on distance-based correspondence with the point-to-plane ICP [18]. In the coarse registration, we find a single transformation applied to all teeth; in the fine registration, we compute individual transformations for each tooth. Point-to-plane ICP leverages the surface normal of the objects and has better convergence and performance than vanilla ICP with a proper initial alignment [19]. In our case, the initial alignment based on centroid alignment helped point-to-plane ICP perform well. During the coarse registration, we used IOS as the target, and CBCT as source. The correspondence and objective in a single ICP iteration are defined as follows. $\mathrm{Corr}(y) := \underset{x \in X_i}{\arg\min} \|y - x\|$ for $y \in Y_i$, and

$$R^{\text{coarse}} = \underset{R}{\arg\min} \quad \sum_{i=1}^{n} \sum_{y \in Y_i} \|(R(\mathrm{Corr}(y)) - y) \cdot n_{\mathrm{Corr}(y)}\|^2 \tag{2}$$

where $n_{\mathrm{Corr}(y)}$ denotes the surface normal for point $\mathrm{Corr}(y)$.

3) Fine Registration: The fine registration finds the transformation for individual teeth, mainly to mitigate stitching errors in IOS. The intraoral scanner sequentially captures dental structures, merging them into a single image, which leads to cumulative stitching errors [8]. We consider registration of teeth in groups similar to [14]. We form a consecutive group of three neighboring teeth. If we denote a group as a set of three tooth numbers, there are $n-2$ groups given by $\{1,2,3\}, \{2,3,4\}, \ldots, \{n-2, n-1, n\}$. The registration is done for each group; as a result, the effect of cumulative stitching errors will be small, but the neighboring teeth help stabilize the alignment of the center tooth.

We consider a novel *sequential correction* scheme as follows. Let us denote the ith group as G_i where $G_i = \{i-1, i, i+1\}$. The registration of $G_2, G_3, \ldots, G_{n-1}$ are done *in sequence*, meaning that registration results of G_{i-1} propagates to G_i, and so on. The idea is that the correction made in a group will help reduce stitching errors in the neighboring group. This is analogous to sequential filtering with a sliding window of length 3. Since the stitching errors are present in IOS, we designate IOS as the source and CBCT as the target during the iteration of point-to-plane ICP. The registration objective for group G_i can be shown to be

$$R_i^{\text{fine}} = \underset{R}{\arg\min} \quad \sum_{y \in Y_{i-1}^i \cup Y_i^i \cup Y_{i+1}^i} \|(R(y) - \mathrm{Corr}(y)) \cdot n_y\|^2 \tag{3}$$

where $Y_i^j := \{R_{j-1}^{\text{fine}}(y) | y \in Y_i^{j-1}\}$ for $j = i, i+1$ and $Y_i^{i-1} := Y_i$. Thus, the points in Y_i is applied with composite transformation $R_{i+1}^{\text{fine}} \circ R_i^{\text{fine}} \circ R_{i-1}^{\text{fine}}$, and such multiple corrections can enhance the registration accuracy.

2.3 Crown removal and Mesh stitching

1) Crown Removal: To replace the crown, we first remove the crown portion of the CBCT. We first identify the *boundary points* of IOS mesh which are

defined as a sequence of points that define a path in the graph induced by vertices and edges along the boundary (cutoff of tooth from gingiva) of the IOS mesh. As we traverse the path, the CBCT points near the path vertices are identified. Those points in CBCT are interconnected via Dijkstra's algorithm [7] to create a short path on the graph induced by the CBCT mesh. The mesh is then split into parts based on the path, and the crown part is removed. There are additional algorithmic details in the removal, and its pseudocode is provided in the supplementary materials.

2) Mesh Stitching: After removing the crown part of CBCT, we stitch the crown from the IOS mesh and the root from the CBCT mesh. The stitching algorithm consists of three parts: 1) Mesh Generation, 2) Intermediate Point Generation, 3) Interpolate Points. A pseudocode is given in Algorithm 1.

Algorithm 1 Integrated Mesh Generation

Require: N: neighbor count, K: degree of interpolation, m: iteration count

1: **function** MeshGeneration(IOS, CBCT, numTeeth, N, K, m):
2: **for** $i \leftarrow 1$ **to** numTeeth **do**
3: $\text{IOS}_i \leftarrow$ Boundary points of IOS tooth number i
4: $\text{CBCT}_i \leftarrow$ Boundary points of CBCT tooth number i
5: midMesh $\leftarrow$ GenInterPoints($\text{IOS}_i, \text{CBCT}_i, N, K, m$)
6: midMesh $\leftarrow$ DownSample(midMesh)
7: $\text{resultMesh}_i \leftarrow$ Delaunay3D(midMesh)
8: **return** array of resultMesh

9: **function** GenInterPoints(A, B, N, K, m):
10: **if** $m = 0$ **then**
11: **return** empty array with dimensions of A
12: ptsMid $\leftarrow$ InterpolatePoints(A, B, N, K)
13: pts$A \leftarrow$ GenInterPoints(A, ptsMid, $N, K, m-1$)
14: pts$B \leftarrow$ GenInterPoints(ptsMid, $B, N, K, m-1$)
15: **return** Concat(pts$A$, ptsMid, pts$B$)

16: **function** InterpolatePoints(A, B, N, K):
17: Initialize empty array interpolatedPoints
18: Create KD-tree from B
19: **for** each point in A **do**
20: Find N nearest neighbors from B using KD-tree
21: **for** each neighbor **do**
22: Calculate K interpolated points between current point and neighbor
23: Add each interpolated point to interpolatedPoints
24: **return** interpolatedPoints

Mesh Generation: This is the top-level function that takes IOS and CBCT inputs and generates intermediate points, i.e., calls function GenInterPoints (line 5) to fill the gap between IOS and CBCT boundaries. After the point

generation, the voxel downsampling with 0.05 mm is applied to the generated point cloud (line 6) to control the point density as appropriate for meshing.
Intermediate Point Generation: Function GenInterPoints is key to the proposed mesh stitching. The function recursively generates the intermediate points in the boundary gap as follows. Given the initial boundary points of IOS and CBCT, the function generates ptsMid between IOS and CBCT via interpolation (line 12). Then the function recursively fills the gap between IOS and ptsMid (line 13), and then ptsMid and CBCT (line 14).
Interpolate Points: Function InterpolatePoints creates the intermediate points given two point sets via interpolation. It uses a KD-tree for efficient neighbor search and point correspondence between two sets (line 18). Following the correspondence through N-nearest neighbor, K interpolation points are generated on the line segment connecting the corresponding points (lines 20-23).

In summary, the proposed stitching can effectively create meshes to smoothly fill the gap between input meshes (Fig. 1(b)) through recursive point generation/interpolation and downsampling.

3 Experiment

3.1 Dataset

The dataset consisted of 62 anonymized pairs of CBCT and IOS collected from the Korea University Anam Hospital. This study was approved by the Institutional Review Board of the same hospital (IRB No. 2020AN0410). The dimension of CBCT images is $768 \times 768 \times 576$ with the voxel size $0.3 \times 0.3 \times 0.3\text{mm}^3$. The IOS scanner was Medit i500 with an in vivo resolution of 50μm. The teeth in the CBCT and IOS datasets were individually labeled by two experts and confirmed by an oral and maxillofacial surgeon. In the experiments, we used the annotated CBCT and IOS as the segmented inputs to our method.

3.2 Experimental Results

We evaluated the registration accuracy at each stage based on a surface distance between IOS and CBCT points in Table 1(a). For the method by Jang *et al.* [14] which is the current state-of-the-art, none of the image pairs in the dataset were properly aligned due to unsuccessful FPFH feature matching, as indicated by '-' in the first entry of Table 1(a) (a failure case is provided in the supplementary materials). For comparison, Jang *et al.*'s method was divided into stages and combined with our centroid alignment. Overall, Table 1(a) shows that our method achieved significantly higher accuracy, which is perhaps due to the synergistic effect of combining centroid alignment and point-to-plane ICP, whereas Jang *et al.*'s vanilla ICP and FPFH matching [14] require a tight initial alignment between objects. Moreover, the sequential error correction by the fine registration (FR) makes further improvement, as can be observed in Table 1(a) by the reduction in error by adding the FR component to our method.

Table 1. (a) Comparison of registration methods in SD (Surface Distance) error. CA: Centroids Alignment (Ours), CR: Coarse Registration (Ours), FR: Fine Registration (Ours), LR: Local Refinement [14], SEC: Stitching Error Correction [14], (b) Quality assessment by experts for CBCT-only and fused modalities.(Score: 1-5)

Method	SD (mm)
Jang *et al.* [14]	-
CA	1.1486
CA +LR [14]	0.5591
CA +LR +SEC [14]	0.4244
CA +CR	0.2540
Ours (CA+CR+FR)	**0.2318**

(a)

	CBCT only	**Modality Fusion**
Incisor	2.571	**3.929**
Canine	2.393	**3.893**
Premolar	2.286	**4.679**
Molar	2.250	**4.607**

(b)

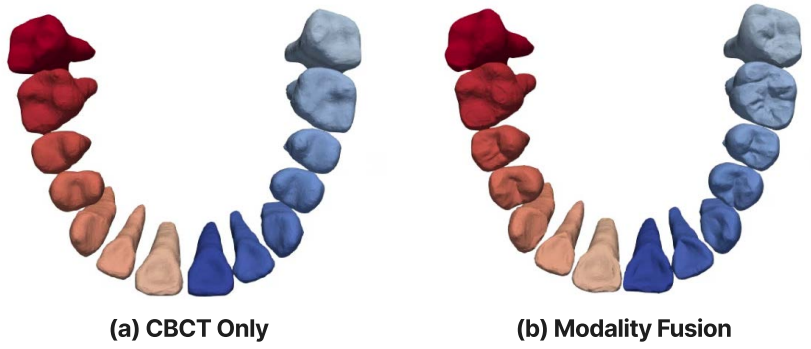

Fig. 2. Comparison of Overall Teeth Structure

Next, we present qualitative evaluations of the integrated outputs. Fig. 2 presents an overall visualization of CBCT-only and integrated IOS and CBCT. While preserving the positional relationship of the teeth, modality fusion provides a much higher resolution in the crown images. Fig. 3 provides a qualitative comparison by tooth types. In all types, modality fusion exhibits significantly enhanced precision in the crown representation. This is particularly evident in Premolars and Molars, for which CBCT imaging often results in poor precision at the contact surface due to the tight spacing between upper and lower teeth during the image acquisition. Fig. 4 shows that our output in unified mesh appears natural and smooth, and restores intricate anatomical details of the crown. However, the method by Qian *et al.* [20] produces incomplete stitching, perhaps due to the large discrepancy in point densities between IOS and CBCT.

Finally, we present the evaluation results from the medical experts. Table 1 (b) presents the assessment scores on sample outputs in a 5-point Likert scale received independently from 7 dental experts. The score represents the overall quality with a focus on *clinically accurate representation*: 5 is the highest and 1 is the lowest rating. The modality fusion achieved significantly higher ratings across all

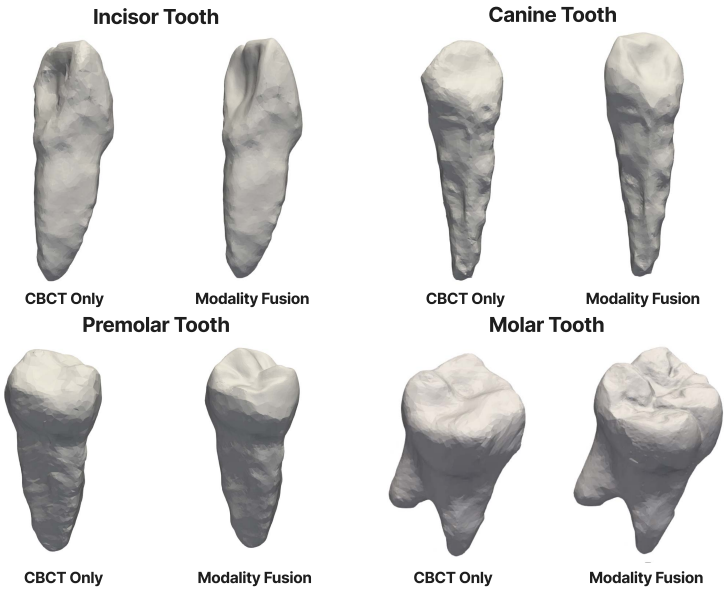

Fig. 3. Comparison of Incisor, Canine, Premolar and Molar Tooth

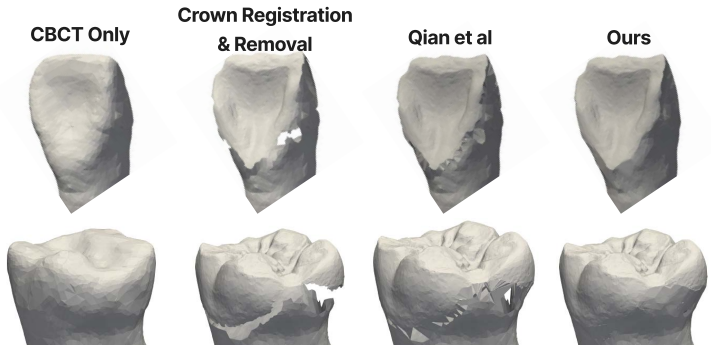

Fig. 4. Comparison of Mesh Stitching Algorithm

tooth types than CBCT-only, particularly in premolars and molars. The overall assessment by experts reads: *"Overall, the results for teeth with modality fusion were superior, especially in premolars and molars where anatomical details such as marginal ridges, cusps, and fissures were well-preserved."*

4 Conclusion

In this paper, we proposed a method for fully automated registration and mesh stitching for a multimodal integration of CBCT and IOS data. We developed

a coarse-to-fine registration strategy, mesh removal, and stitching to bridge the modality gap, producing a single mesh output with high quality and accuracy. Our advancement enables enhanced precision for many applications such as virtual surgeries for personalized patient care through AR/XR technologies. Future work includes extending and verifying the proposed framework on diverse datasets varying in spatial resolution, image artifacts, patient conditions, etc.

Acknowledgements. This research was supported by the National Research Foundation of Korea (NRF) grant funded by the Korea government (MSIT) (No. No.2022R1A5A1027646), the MSIT (Ministry of Science and ICT), Korea, under the ICT Creative Consilience program (IITP-2020-0-01819) supervised by the IITP (Institute for Information & communications Technology Planning & Evaluation), and the Korea Medical Device Development Fund grant funded by the Korea government (the Ministry of Science and ICT, the Ministry of Trade, Industry and Energy, the Ministry of Health & Welfare, the Ministry of Food and Drug Safety) (Project Number: 1711195279 , RS-2021-KD000009).

Disclosure of Interests

The authors have no competing interests to declare that are relevant to the content of this article.

References

1. Besl, P.J., McKay, N.D.: Method for registration of 3-d shapes. In: Sensor fusion IV: control paradigms and data structures. vol. 1611, pp. 586–606. Spie (1992)
2. Chung, M., Lee, J., Song, W., Song, Y., Yang, I.H., Lee, J., Shin, Y.G.: Automatic registration between dental cone-beam ct and scanned surface via deep pose regression neural networks and clustered similarities. IEEE Transactions on Medical Imaging **39**(12), 3900–3909 (2020)
3. Cui, Z., Fang, Y., Mei, L., Zhang, B., Yu, B., Liu, J., Jiang, C., Sun, Y., Ma, L., Huang, J., et al.: A fully automatic ai system for tooth and alveolar bone segmentation from cone-beam ct images. Nature communications **13**(1), 2096 (2022)
4. Cui, Z., Li, C., Chen, N., Wei, G., Chen, R., Zhou, Y., Shen, D., Wang, W.: Tsegnet: An efficient and accurate tooth segmentation network on 3d dental model. Medical Image Analysis **69**, 101949 (2021)
5. Cui, Z., Li, C., Wang, W.: Toothnet: automatic tooth instance segmentation and identification from cone beam ct images. In: Proceedings of the IEEE/CVF Conference on Computer Vision and Pattern Recognition. pp. 6368–6377 (2019)
6. Deferm, J., Nijsink, J., Baan, F., Verhamme, L., Meijer, G., Maal, T.: Soft tissue-based registration of intraoral scan with cone beam computed tomography scan. International Journal of Oral and Maxillofacial Surgery **51**(2), 263–268 (2022)
7. Dijkstra, E.W.: A note on two problems in connexion with graphs. In: Edsger Wybe Dijkstra: His Life, Work, and Legacy, pp. 287–290 (2022)
8. Ender, A., Zimmermann, M., Mehl, A.: Accuracy of complete-and partial-arch impressions of actual intraoral scanning systems in vitro. International journal of computerized dentistry **22**(1), 11–19 (2019)

9. Ezhov, M., Gusarev, M., Golitsyna, M., Yates, J.M., Kushnerev, E., Tamimi, D., Aksoy, S., Shumilov, E., Sanders, A., Orhan, K.: Clinically applicable artificial intelligence system for dental diagnosis with cbct. Scientific reports **11**(1), 15006 (2021)
10. Gateno, J., Xia, J., Teichgraeber, J.F., Rosen, A.: A new technique for the creation of a computerized composite skull model. Journal of oral and maxillofacial surgery **61**(2), 222–227 (2003)
11. Hao, J., Liu, J., Li, J., Pan, W., Chen, R., Xiong, H., Sun, K., Lin, H., Liu, W., Ding, W., et al.: Ai-enabled automatic multimodal fusion of cone-beam ct and intraoral scans for intelligent 3d tooth-bone reconstruction and clinical applications. arXiv preprint arXiv:2203.05784 (2022)
12. Hung, K., Yeung, A.W.K., Tanaka, R., Bornstein, M.M.: Current applications, opportunities, and limitations of ai for 3d imaging in dental research and practice. International Journal of Environmental Research and Public Health **17**(12), 4424 (2020)
13. Hyun, C.M., Bayaraa, T., Yun, H.S., Jang, T.J., Park, H.S., Seo, J.K.: Deep learning method for reducing metal artifacts in dental cone-beam ct using supplementary information from intra-oral scan. Physics in Medicine & Biology **67**(17), 175007 (2022)
14. Jang, T.J., Yun, H.S., Hyun, C.M., Kim, J.E., Lee, S.H., Seo, J.K.: Fully automatic integration of dental cbct images and full-arch intraoral impressions with stitching error correction via individual tooth segmentation and identification. arXiv preprint arXiv:2112.01784 (2021)
15. Kim, S., Song, I.S., Baek, S.J.: Automatic segmentation of internal tooth structure from cbct images using hierarchical deep learning. In: International Conference on Medical Image Computing and Computer-Assisted Intervention. pp. 703–713. Springer (2023)
16. Liang, Y., Qiu, L., Lu, T., Fang, Z., Tu, D., Yang, J., Shao, Y., Wang, K., Chen, X., He, L.: Oralviewer: 3d demonstration of dental surgeries for patient education with oral cavity reconstruction from a 2d panoramic x-ray. In: 26th International Conference on Intelligent User Interfaces. pp. 553–563 (2021)
17. Liu, J., Hao, J., Lin, H., Pan, W., Yang, J., Feng, Y., Wang, G., Li, J., Jin, Z., Zhao, Z., et al.: Deep learning-enabled 3d multimodal fusion of cone-beam ct and intraoral mesh scans for clinically applicable tooth-bone reconstruction. Patterns **4**(9) (2023)
18. Low, K.L.: Linear least-squares optimization for point-to-plane icp surface registration. Chapel Hill, University of North Carolina **4**(10), 1–3 (2004)
19. Pomerleau, F., Colas, F., Siegwart, R., Magnenat, S.: Comparing icp variants on real-world data sets: Open-source library and experimental protocol. Autonomous robots **34**, 133–148 (2013)
20. Qian, J., Lu, S., Gao, Y., Tao, Y., Lin, J., Lin, H.: An automatic tooth reconstruction method based on multimodal data. Journal of Visualization **24**, 205–221 (2021)
21. Singhal, I., Kaur, G., Neefs, D., Pathak, A.: A literature review of the future of oral medicine and radiology, oral pathology, and oral surgery in the hands of technology. Cureus **15**(9) (2023)
22. Sukotjo, C., Schreiber, S., Li, J., Zhang, M., Chia-Chun Yuan, J., Santoso, M.: Development and student perception of virtual reality for implant surgery. Education Sciences **11**(4), 176 (2021)

23. Swennen, G., Barth, E.L., Eulzer, C., Schutyser, F.: The use of a new 3d splint and double ct scan procedure to obtain an accurate anatomic virtual augmented model of the skull. International journal of oral and maxillofacial surgery **36**(2), 146–152 (2007)
24. Swennen, G., Mommaerts, M., Abeloos, J., De Clercq, C., Lamoral, P., Neyt, N., Casselman, J., Schutyser, F.: A cone-beam ct based technique to augment the 3d virtual skull model with a detailed dental surface. International journal of oral and maxillofacial surgery **38**(1), 48–57 (2009)
25. Wang, H., Minnema, J., Batenburg, K.J., Forouzanfar, T., Hu, F.J., Wu, G.: Multiclass cbct image segmentation for orthodontics with deep learning. Journal of dental research **100**(9), 943–949 (2021)
26. Xia, J.J., Gateno, J., Teichgraeber, J.F.: New clinical protocol to evaluate craniomaxillofacial deformity and plan surgical correction. Journal of Oral and Maxillofacial Surgery **67**(10), 2093–2106 (2009)
27. Xiong, H., Li, K., Tan, K., Feng, Y., Zhou, J.T., Hao, J., Ying, H., Wu, J., Liu, Z.: Tsegformer: 3d tooth segmentation in intraoral scans with geometry guided transformer. In: International Conference on Medical Image Computing and Computer-Assisted Intervention. pp. 421–432. Springer (2023)
28. Zhao, Y., Zhang, L., Liu, Y., Meng, D., Cui, Z., Gao, C., Gao, X., Lian, C., Shen, D.: Two-stream graph convolutional network for intra-oral scanner image segmentation. IEEE Transactions on Medical Imaging **41**(4), 826–835 (2021)
29. Zhou, X., Gan, Y., Xiong, J., Zhang, D., Zhao, Q., Xia, Z.: A method for tooth model reconstruction based on integration of multimodal images. Journal of healthcare engineering **2018** (2018)